Journal of
Synchrotron
Radiation

ISSN 0909-0495

Received 24 October 2011
Accepted 4 December 2011

Modular deposition chamber for *in situ* X-ray experiments during RF and DC magnetron sputtering

Bärbel Krause,[a]* Susan Darma,[a] Marthe Kaufholz,[a] Hans-Hellmuth Gräfe,[a] Sven Ulrich,[b] Miguel Mantilla,[c] Ralf Weigel,[c] Steffen Rembold[d] and Tilo Baumbach[a]

[a]ANKA, Institut für Synchrotronstrahlung, Karlsruher Institut für Technologie, Karlsruhe, Germany, [b]Institut für Angewandte Materialien, Angewandte Werkstoffphysik, Karlsruher Institut für Technologie, Karlsruhe, Germany, [c]Max-Planck-Institut für Intelligente Systeme, Stuttgart, Germany, and [d]CreaTec Fischer and Co. GmbH, Erligheim, Germany.
E-mail: baerbel.krause@kit.edu

A new sputtering system for *in situ* X-ray experiments during DC and RF magnetron sputtering is described. The outstanding features of the system are the modular design of the vacuum chamber, the adjustable deposition angle, the option for plasma diagnostics, and the UHV sample transfer in order to access complementary surface analysis methods. First *in situ* diffraction and reflectivity measurements during RF and DC deposition of vanadium carbide demonstrate the performance of the set-up.

© 2012 International Union of Crystallography
Printed in Singapore – all rights reserved

Keywords: *in situ* X-ray measurement; thin-film growth; sputter deposition; deposition chamber; texture; polycrystalline materials.

1. Introduction

In situ X-ray studies during thin-film deposition are an extremely useful tool for the investigation of structure formation processes on the atomic and microscopic scale, thus helping to understand the interplay between the microstructure and macroscopic coating properties. The method can be applied to very different deposition techniques, such as molecular beam epitaxy (Jenichen *et al.*, 2003; Renaud *et al.*, 2004), pulsed laser deposition (Willmott *et al.*, 2005; Vonk *et al.*, 2005) or metal-organic vapour phase epitaxy (Fuoss *et al.*, 1995). One deposition technique which is used for a wide range of industrial applications is reactive and non-reactive magnetron sputtering. Each application requires a distinct optimized coating structure, varying from amorphous layers up to large well aligned crystallites. Zone models have been developed to describe the influence of the process parameters on the morphology and microstructure formation (Thornton, 1974; Mahieu *et al.*, 2006; Anders, 2010). However, the structure formation process is still not well understood. One reason is the complex relation between the accessible process parameters and the plasma parameters which determine the microstructure (Kersten *et al.*, 2001; Han, 2009). Another reason is the complexity of the growth process itself, which makes high demands not only on the experimental growth studies but also on the simulation tools. Only a combined approach using complementary *in situ* and *ex situ* thin-film and surface analysis methods together with comprehensive growth simulations can lead to a detailed understanding of the structure formation.

Several sputtering systems for *in situ* X-ray experiments during thin-film deposition are reported in the literature. Most chambers were designed for synchrotron radiation diffraction and refraction experiments (Zheng *et al.*, 1991; Payne *et al.*, 1993; Williams *et al.*, 1991; Matz *et al.*, 2001; Peverini *et al.*, 2005; Liang *et al.*, 2007; Schell *et al.*, 2007). However, chambers for laboratory X-ray sources can also be found (Lützenkirchen-Hecht *et al.*, 2005), as well as chambers for other X-ray methods such as X-ray absorption spectroscopy (Ringpfeil *et al.*, 2007), X-ray magnetic circular dichroism (Telling *et al.*, 2006) and energy-dispersive X-ray diffraction (Ellmer *et al.*, 2001). The chambers have in common that they are optimized for X-ray experiments and make a compromise on some features desired for a growth-optimized chamber. Unfortunately, the plasma parameters are not determined, and complementary methods are only available after exposing the sample to ambient conditions.

The sputtering system described here is one approach to overcoming these limitations. The system is stationed in the UHV analysis laboratory of the Angstrømquelle Karlsruhe (ANKA), in direct neighbourhood with the beamlines. It is designed for the study of amorphous and polycrystalline thin films and multilayers deposited by reactive and non-reactive sputtering. Both DC and RF magnetron sputtering are available, thus extending the range of materials which can be deposited by non-reactive sputtering. The chamber is suited to

various X-ray methods, including reflectivity measurements giving information about roughness, density and film thickness; wide-angle X-ray scattering measurements sensitive to the crystalline structure, crystallite size and texture; and grazing-incidence X-ray absorption spectroscopy measurements for the study of the short-range order. Owing to the modular design of the chamber, several growth geometries can be realised. The possiblilty for UHV sample transfer to other vacuum systems gives access to complementary analysis methods.

In the following, the sputtering system and its measurement capabilities are described in detail. The design of the chamber and the experimental set-up are summarized in §2. First *in situ* measurements are presented in §3, followed by the conclusions and outlook in §4.

2. Technical description of the system

Our sputtering system consists of a UHV-compatible vacuum chamber, a gas panel and a rack containing the power supplies, controllers and an industrial PC. One central feature of the system is the modular concept of the sputtering chamber itself. The chamber can be used in alternative configurations, thus overcoming spatial limitations and extending the experimental possibilities. In the following, the functionalities of the system are described in detail.

2.1. Design of the sputtering chamber

The design of an *in situ* sputtering chamber combines the requirements of a growth chamber with the demands of an X-ray experiment. Many industrial sputtering chambers employ the coaxial geometry, *i.e.* the surface of the sputter target is parallel to the sample surface. Combining this geometry with the X-ray experiment, the accessible angular range is cylindrical, limited to small incident angles by the sample horizon and to large incident angles by the magnetron source. We have based our sputtering chamber on this geometry, with the additional demand that the chamber should be compatible with the UHV cluster system situated in the ANKA UHV analysis laboratory. Furthermore, the distance between the mounting table of the diffractometer and the sample position should not exceed 170 mm, in order to be compatible with most heavy load diffractometer set-ups.

The cylindrical body of the vacuum chamber consists of three exchangeable sections (see Fig. 1) which are based on a CF 200 flange. The growth-related components such as pumping system, magnetron sources, pressure measurement and sample manipulator are mounted in the top and base part, separated from the X-ray window and the sample transfer in the center part. Fig. 1 summarizes the presently available components, which are one top part with two alternative sputtering source configurations [Figs. 1(*a*) and 1(*b*)], two alternative center parts with and without beryllium window [Figs. 1(*c*) and 1(*d*)], and two alternative base parts with different sample manipulators [Figs. 1(*e*) and 1(*f*)].

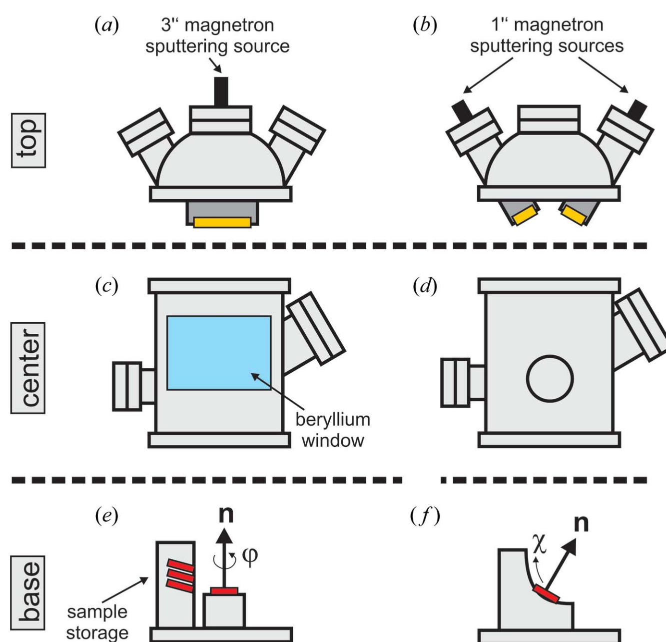

Figure 1
Modular concept of the vacuum chamber. The chamber consists of three exchangeable segments which can be combined according to the needs of the experimentalist (for details see text).

In standard configuration for coaxial growth geometry (see Fig. 2), the weight of the chamber is about 60 kg. A UHV magnetron sputtering source for targets of diameter 3 inch and maximum thickness 8 mm (ION'X-3"UHV_9200_CF100, Thin Film Consulting) is mounted on the central CF 100 flange of the top part (Fig. 1*a*). The substrate is mounted on the rotation manipulator shown in Fig. 1(*e*) which allows for a motorized sample rotation around the surface normal by 320° and is equipped with a resistive heater for temperatures up to

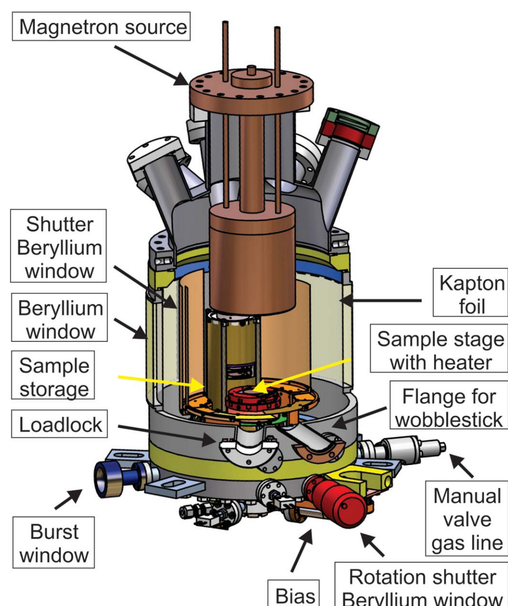

Figure 2
Configuration of the sputtering chamber for coaxial growth geometry.

1173 K. In this configuration the target–substrate distance is 120 mm. Two type-K sheath thermocouples are installed, one measuring the temperature close to the sample and a reference thermocouple for temperature calibration which can be mounted directly at the sample position. RF or DC bias can be applied *via* a pneumatically actuated stamp. During sample rotation the stamp is retracted.

Alternatively, for example for multilayer growth, two 1 inch UHV magnetron sputtering sources with chimney (AJA International, type 310-XP-UA) can be mounted on CF 40 flanges tilted by 22° from the sample surface normal (Fig. 1*b*). In this configuration the distance between target and substrate surface is 100 mm. The influence of the tilt angle on the texture development can be studied in detail using the tilt manipulator (Fig. 1*f*). This manipulator has similar bias and heating possibilities as the rotation manipulator, but allows for a motorized sample tilt between horizontal and vertical geometry.

The standard sample holder used in the sputtering chamber is optimized for samples with a maximum lateral size of 25 mm and a typical thickness of 1–2 mm. It is compatible with the UHV transfer system in the UHV analysis laboratory. Larger samples with a maximum diameter of about 100 mm can be mounted on a special adapter plate which is incompatible with the UHV transfer.

For sample transfer, a CF 40 valve serving as load lock, a wobble stick and a CF 63 window are installed in the center part of the chamber. A manual shutter protects the windows against coating; RF leakage is prevented by a metal grid. For better visibility of the transfer, a lamp is mounted in the top part of the chamber. To minimize the unproductive time during growth experiments, a sample storage for five transfer plates, well shielded from sputtered material, is mounted on the base part with rotation manipulator [see Fig. 1(*e*)]. The wobble stick is used for the transfer between manipulator and sample storage.

A Langmuir probe with motorized probe position is available for plasma diagnostics. It can be mounted on the load lock or the flange of the wobble stick. Important plasma parameters such as the plasma potential, the electron energy distribution function and the ion and electron densities can be determined. In collaboration with the Institut für Angewandte Materialien – Angewandte Werkstoffphysik (IAM–AWP) of the KIT, other plasma diagnostics tools such as retarding field analyzer, Faraday cup, double probe and optical emission spectroscopy can also be employed.

Two large beryllium windows with a thickness of 0.5 mm and a purity of 99% are directly welded to the center part of the chamber. The windows cover an azimuthal angle of −50° to +65°. The maximum angle between sample surface and incident or scattered beam is 44°. The angular range of the windows allows large areas of reciprocal space to be measured simultaneously and with good time resolution using a two-dimensional detector. Standard scattering methods such as reflectivity measurements, grazing-incidence X-ray diffraction, crystal truncation rod measurements, coplanar and specular diffraction can be performed with a wide angular range.

For protection against coating, the Be windows are covered by an exchangeable Kapton foil. Owing to the low absorption of the Be windows and the Kapton foil, the sample environment does not significantly reduce X-ray scattering or the fluorescence signal of the sample. At an X-ray energy of 5.5 keV, the transmission is reduced to $T = 0.5$. Typically, the experiments will be performed in the energy range 8–12 keV where a transmission between $T = 0.79$ and $T = 0.92$ is expected.

For growth experiments in the laboratory where no X-ray transparency is required, an additional stainless steel shutter actuated by a rotary feedthrough can be moved manually in front of the Be windows. Optionally a center part without Be window [see Fig. 1(*d*)] can be installed offering several CF 40 flanges for additional components, *e.g.* for plasma diagnostics.

The pumping system of the chamber consists of a turbo pump (HighPace 300, Pfeiffer Vacuum) and a membrane pump (Vacuubrand). During thin-film deposition, the pumping speed can be regulated with a motorized throttling valve. A flexible bellow is installed between the top part of the chamber and the turbo pump so that the turbo pump can be mounted independently. The chamber is equipped with two systems for pressure measurement: a cold cathode for wide-range pressure measurement and a baratron for pressures larger than 10^{-4} mbar during deposition. Since the baratron orientation should not be changed during measurement, it is decoupled from the chamber by a flexible bellow. After bakeout, the base pressure of the system is about 6×10^{-9} mbar; without bakeout a pressure of 1×10^{-8} mbar has been observed.

The sputter gases enter the base part of the growth chamber through a common gas inlet with manual valve. The gas mixture required for reactive or non-reactive sputtering is adjusted on a separate gas panel with three independent gas inlets. Each gas inlet is connected to two mass flow controllers for low and high flux (MKS; flow range 0–10 sccm and 0–50 sccm).

The sputtering process is fully automated using customized visualization software from Diener Automation. The automation allows complex growth recipes under controlled and reproducible conditions to be realised. The process parameters including the manipulator position, the substrate temperature, the gas flow, the pressure in the chamber and the output parameters of the power supplies (incident and reflected power, voltage and current) are visualized in real time during the experiment. The maximum data acquisition rate is 1 point per 100 ms. Since this high rate is not required for our experiments, the data are typically logged with one data point per second. They can be accessed by other computers, *e.g.* for synchronizing the X-ray experiments with the growth process.

2.2. Laboratory and beamline set-up

Similar to a standard sputtering system, our portable system can be operated in a laboratory environment [see Fig. 3(*a*)]. The UHV analysis laboratory with its stationary UHV cluster

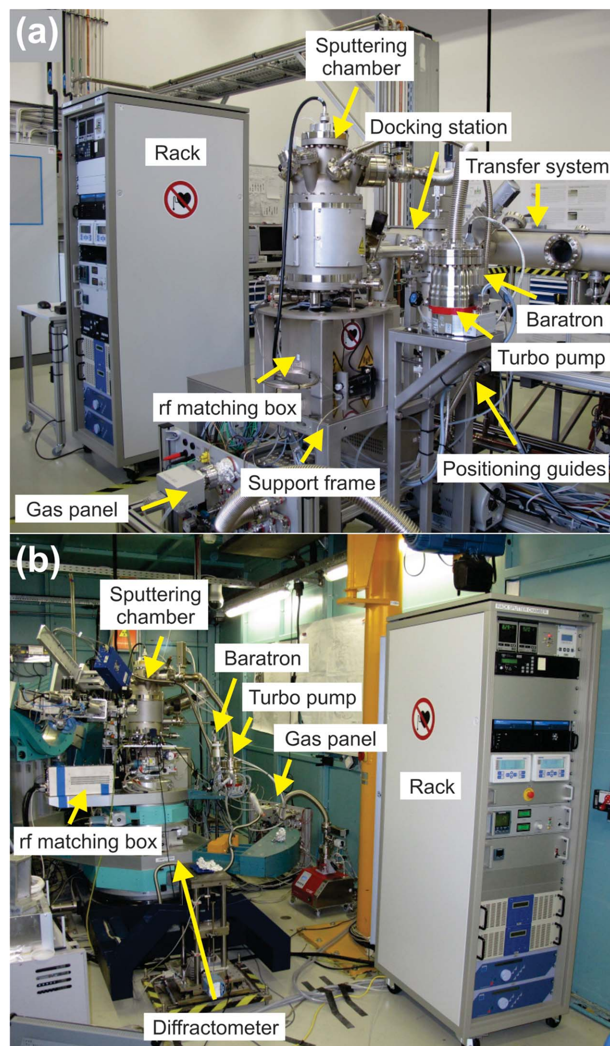

Figure 3
(*a*) Sputtering system in the ANKA UHV analysis laboratory; (*b*) sputtering system installed at the ANKA MPI beamline.

is situated in the ANKA hall, close to the beamlines. The sputtering chamber can be attached to the UHV cluster, thus having access to complementary UHV surface analysis methods such as X-ray photoelectron spectroscopy and scanning probe microscopy. In the laboratory, deposition rates are calibrated, the plasma parameters are characterized and time-consuming systematic growth studies are performed as preparation for the *in situ* X-ray experiments. For the *in situ* X-ray experiments the sputtering system can be temporarily installed at various ANKA beamlines equipped for heavy load and large sample environments, including the beamlines NANO, Pdiff, MPI and XAS. Fig. 3(*b*) shows the experimental set-up at the MPI beamline. In the following the different set-ups as well as the transfer from one set-up to another are summarized.

In the laboratory set-up shown in Fig. 3(*a*) the sputtering chamber is mounted vertically on a stainless steel support frame, forming one unit together with the gas panel, the RF matching boxes, the turbo pump and the baratron. This unit can be docked *via* an intermediate pumping chamber to the transfer system of the UHV analysis cluster. Mechanical guides are installed for reproducible positioning of the chamber during the docking process. The sample transfer takes place with an adjustable transfer rod mounted on the UHV analysis cluster. The gas panel is connected to the argon and nitrogen gas lines of the cluster. A gas cabinet is available for storage of additional gases. For bakeout of the sputtering chamber a rigid bakeout box can be installed on the support frame.

In the beamline set-up shown in Fig. 3(*b*), the vacuum chamber is mounted vertically or horizontally on the diffractometer, the gas panel is installed as close as possible to the chamber while the rack can be placed further away. The short distance between chamber and gas panel minimizes the required length of the gas line, thus improving the switching time of the gas flow. The turbo pump, the baratron and the RF matching boxes are placed close to the chamber but not on the goniometer itself. The baratron should not be tilted during operation, and both matching boxes and turbo pump would increase the weight and the space requirements of the chamber significantly, thus reducing the flexibility of the system. During the *in situ* X-ray experiments, the growth process is remote-controlled from the beamline control cabin.

During the transfer between laboratory and beamline, the vacuum of the chamber is maintained but the pumps are switched off for about 2 h. Reconnecting all cables, gas lines and cooling water pipes takes about one day because special care has to be taken that the cabling does not hinder the diffractometer movements.

3. First *in situ* measurements

For epitaxial thin films, reflectivity and crystal truncation rod (CTR) measurements are well established tools for studying the growth mode and material distribution during and after deposition of thin films (Vlieg *et al.*, 1988; Bøttiger *et al.*, 2002; Kaganer *et al.*, 2004). In the case of polycrystalline and textured coatings, no long-range lateral crystalline order exists and CTR methods cannot be applied. Information about the structural changes during growth is typically derived from the time-dependent changes in the specular reflectivity, the diffuse scattering (Peverini *et al.*, 2005) and the Bragg reflections (Schell *et al.*, 2005).

In situ scattering methods can be divided into scanning methods and measurements at fixed detector position. Scanning methods have a low time-resolution but give very detailed information, while measurements at fixed detector position can be repeated at a high frequency allowing the observation of temporal changes of the coating.

In the following, some examples of *in situ* X-ray scattering experiments feasible with our new sputtering system will be given. As examples for measurements at fixed detector position, time-dependent measurements of the specular reflectivity and the powder diffraction rings will be shown. As examples for scanning methods, the measurement of a large area of reciprocal space and an angle-dependent reflectivity measurement will be presented. From the diffraction

measurements, information about crystalline phases, texture, size and strain of the crystallites can be derived, while the reflectivity measurements give information about the electron density profile of the film which is related to material density, roughness, film thickness and interdiffusion at the interfaces. The time-dependent measurements give insight into the temporal changes of crystalline structure and material distribution during deposition.

3.1. Experimental

The performance of the *in situ* sputtering system was tested at the ANKA MPI beamline, using a monochromatic X-ray beam with energy $E = 10$ keV (corresponding to a wavelength $\lambda = 1.2398$ Å) and a 500 µm × 200 µm (horizontal × vertical) beam size of the focused X-ray beam at the sample position. Several vanadium carbide (VC_{1-x}) coatings were deposited by RF and DC magnetron sputtering on Si(100) substrates. The coatings were deposited from a nominally stoichiometric VC target (Kurt J. Lesker Company). No external heating was employed. The substrates with a lateral size of 20 mm × 20 mm and a thickness of 0.5 mm were covered by natural oxide. The coatings were deposited in coaxial growth geometry. During RF deposition, the gas pressure was regulated to $p = 5 \times 10^{-3}$ mbar and the RF power was 250 W. The measured deposition rate was about 0.05 nm s^{-1}. DC deposition was performed at $p = 1.8 \times 10^{-3}$ mbar with 200 W power, resulting in a deposition rate of about 0.22 nm s^{-1}.

The sputtering chamber was mounted vertically on the diffractometer, *i.e.* the sample surface was horizontal. During deposition, the scattered intensity was detected using a Pilatus detector with an active area of 195 × 487 pixels and a pixel size of 172 µm, mounted at a distance of 400 mm from the sample. For sample aligment an avalanche photodiode was used. Reflectivity measurements were performed using a NaI detector.

3.2. Powder diffraction

Fig. 4(*a*) shows the grazing-incidence wide-angle X-ray scattering (GIWAXS) measured after the DC magnetron sputter deposition of 266 nm VC_{1-x} in two steps of 133 nm. The measurement was performed with the incident angle α_i = 1.6°. Note that it covers only part of the accessible angular range which is not limited by the Be windows but by the specific set-up at the beamline. The image is composed of a series of Pilatus images taken at different detector positions δ (in-plane angle relative to the direct beam) and γ (out-of-plane angle relative to the direct beam) with an integration time of 5 s. The scattered intensity is plotted logarithmically.

Three powder diffraction rings are clearly visible and can be attributed to the (111), (200) and (220) reflections of cubic VC_{1-x}. No indication for hexagonal V_2C was found. Close to $\delta = \gamma = 0$, the specularly reflected beam, a diffuse intensity streak and the diffraction halo of the Kapton foil used as coating protection are visible. Simple geometrical considerations taking into account the distance between detector and sample, the large window size, the chamber diameter and

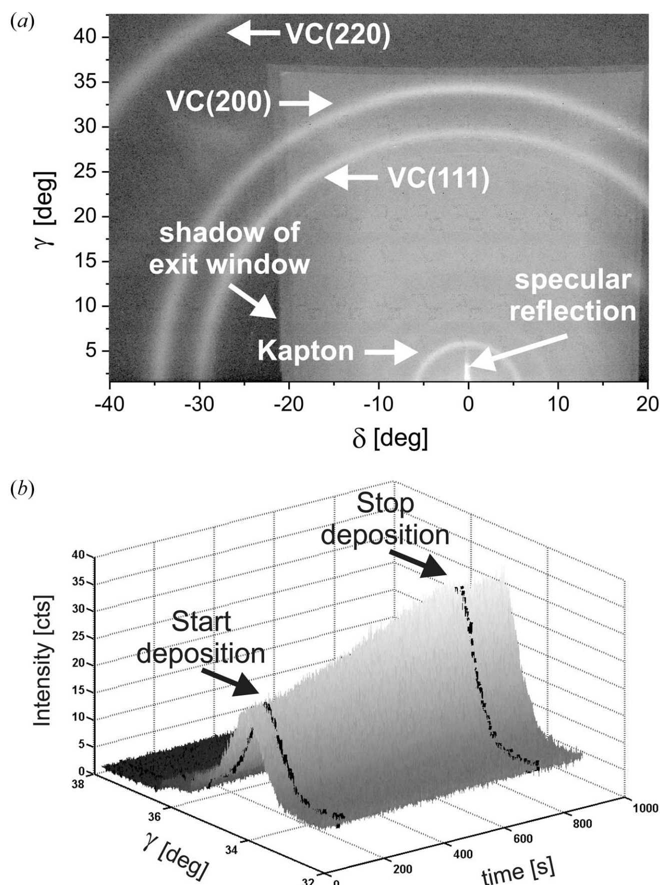

Figure 4
(*a*) Powder diffraction rings of a VC_{1-x} sample deposited by DC magnetron sputtering. (*b*) Time-dependent intensity change of the VC(200) reflection at $\delta = 0°$ measured during the second deposition step.

the positions of various components within the chamber confirmed that the rectangular background intensity distribution is due to the scattering of the incident beam on the entrance Be window. The scattered intensity is partially shadowed by the exit window and its window shutter. Note that the background intensity distribution can change significantly depending on the chamber orientation and configuration.

Owing to the grazing-incidence geometry, the specular direction (normal to the sample surface) which is typically the main texture direction is not accessible. At $\delta = 0$, lattice planes with a tilt angle $\beta = \theta$ between lattice plane normal and surface normal are probed, where θ is the Bragg angle of the respective lattice plane. The powder ring is due to lattice planes with $90° - \alpha_i > \beta > \theta$. For the (111) and (200) reflection, $\beta \simeq 15°$ is still quite close to the surface normal, allowing the study of lateral compression and vertical expansion of the unit cell. Neglecting the strain, the in-plane peak positions of (111) and (200) correspond to a cubic unit cell with lattice parameter $a = 4.19 \pm 0.01$ Å, while the peak positions close to the perpendicular direction (tilted by about 15° from the surface normal) correspond to $a_{111} = 4.24 \pm 0.01$ and $a_{200} = 4.21 \pm 0.01$ Å. The difference between lateral and vertical lattice parameter indicates that the unit cell of the differently

oriented crystallites is deformed owing to the lateral compression of the film, and the deformation seems to be stronger for the (111) oriented crystallites. All measured values are slightly larger than the a = 4.165 Å expected for cubic VC (Nowotny & Kieffer, 1947).

The time-dependent intensity change of the VC(200) reflection at $\delta = 0°$ measured during the second deposition step is shown in Fig. 4(b). For this measurement the Pilatus detector was kept at constant angular position. For each time step the intensity was integrated over the beam width at the detector position. The beginning and end of the deposition are indicated. It is easy to see that the peak intensity increases during deposition.

3.3. Reflectivity

Fig. 5(a) shows the time-dependent specular X-ray intensity at the incident angle α_i = 1.59° during RF magnetron sputtering deposition of 59 nm VC_{1-x}. The intensity is background-corrected and integrated over the specular beam. After an initial intensity increase, regular and only slightly damped intensity oscillations are observed. The oscillations originate from the interference between the X-ray beam reflected at the substrate interface and the X-ray beam reflected at the sample surface. Since the optical path between the two beams changes with increasing film thickness, the measured intensity is sensitive to the time-dependent changes of the film thickness. At α_i = 1.59°, one oscillation period corresponds to an increase of the film thickness by about 2.3 nm. The observed regular oscillations indicate the deposition of a relatively smooth film with constant deposition rate. The damping of the oscillations might be related to a slightly increasing surface roughness with increasing film thickness.

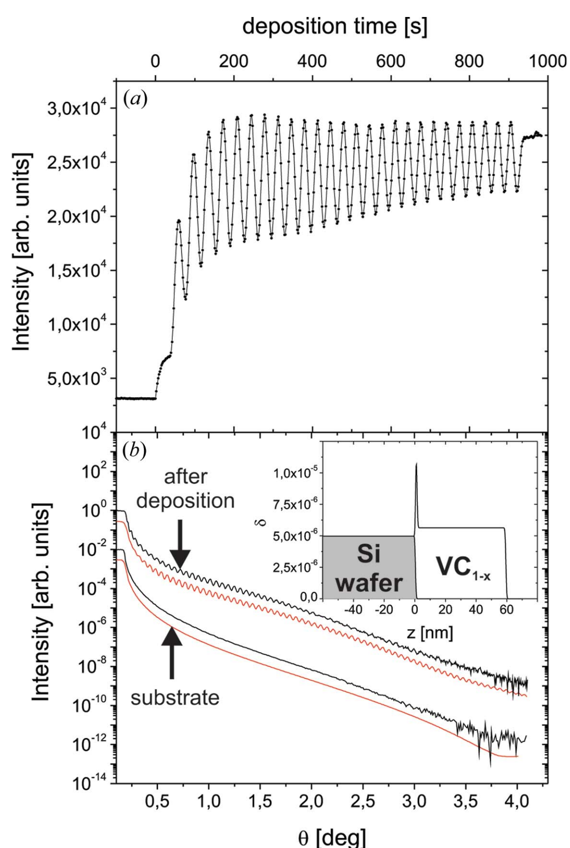

Figure 5
(a) Time-dependent specular X-ray intensity during deposition of 59 nm VC_{1-x}; (b) reflectivity measurement performed before and after deposition (black line). The simulated reflectivity curves [gray line (red online)] are slightly offset; the inset shows the δ-profile used for the fit.

Angle-dependent reflectivity measurements which were performed before and after deposition are shown in Fig. 5(b). After coating, the Kiessig fringes corresponding to the average film thickness are clearly visible. The data were fitted using the software *Parratt32* (Braun *et al.*, 1997), including an experimental resolution of 0.005 $Å^{-1}$. The refraction index for X-rays is $n = 1 - \delta + i\beta$, where δ is proportional to the electron density and β is the absorption correction. The inset of Fig. 5(b) shows the δ-profile used for the fit of the data as a function of z, where $z = 0$ corresponds to the substrate surface. The profile of the substrate (shaded in gray) was used for the fit of both reflectivity scans. δ is constant for almost the entire film thickness and corresponds to about half of the value expected for VC. This indicates a high porosity of the film. Only in a 3 nm layer close to the interface does δ increase almost to the bulk value, as expected for a dense nucleation layer.

4. Conclusions and outlook

A modular sputtering system for *in situ* synchrotron radiation experiments during RF sputtering has been presented. The operation of the chamber was demonstrated, and first experimental results for the growth of VC_{1-x} were presented. The chamber will be used for systematic growth studies of polycrystalline and amorphous materials, combining the study of the plasma parameters with *in situ* X-ray experiments and complementary thin-film analysis methods. Together, these experiments will contribute to an encompassing understanding of the thin-film formation process. Anticipating future demands of the experimentalists, the chamber is compatible with ion–beam etching, ion-beam-assisted deposition, diode sputtering, and base pressures down to 1×10^{-10} mbar.

The authors are grateful for the support of the technical staff at ANKA. They acknowledge the helpful discussions with A. Fischer, R. Diener and C. Diener during the construction of the chamber and the installation of the control system, the discussions about sputtering with Y. Je, and the help from S. Stankov during the ordering phase. The project was financed in the framework of the Excellence Initiative within the project KIT-Nanolab@ANKA.

References

Anders, A. (2010). *Thin Solid Films*, **518**, 4087–4090.
Bøttiger, J., Chevallier, J., Petersen, J. H., Schell, N., Matz, W. & Mücklich, A. (2002). *J. Appl. Phys.* **91**, 5429–5433.

Braun, C. (1997–1999). Copyright Christian Braun, HMI Berlin, Germany.
Ellmer, K., Mientus, R., Weiß, V. & Rossner, H. (2001). *Nucl. Instrum. Methods Phys. Res. A*, **467/468**, 1041–1044.
Fuoss, P. H., Kisker, D. W., Stephenson, G. B. & Brennan, S. (1995). *Mater. Sci. Eng. B*, **30**, 99–108.
Han, J. G. (2009). *J. Phys. D*, **42**, 043001.
Jenichen, B., Braun, W., Kaganer, V. M., Shtukenberg, A. G., Däweritz, L., Schulz, C.-G. & Ploog, K. H. (2003). *Rev. Sci. Instrum.* **74**, 1267–1273.
Kaganer, V., Braun, W. & Ploog, B. J. K. H. (2004). *Surf. Sci.* **560**, 88–102.
Kersten, H., Deutsch, H., Steffen, H., Kroesen, G. M. W. & Hippler, R. (2001). *Vacuum*, **63**, 385–413.
Liang, Y.-C., Lee, H.-Y., Liu, H.-J., Hsieh, Y.-W. & Liang, Y.-C. (2007). *J. Synchrotron Rad.* **14**, 163–168.
Lützenkirchen-Hecht, D., Bruder, K., abd, P., Keil, U. H., Markert, C., Ringpfeil, C. & Frahm, R. (2005). *Rev. Sci. Instrum.* **76**, 073905.
Mahieu, S., Ghekiere, P., Depla, D. & Gryse, R. D. (2006). *Thin Solid Films*, **515**, 1229–1249.
Matz, W., Schell, N., Neumann, W., Bøttiger, J. & Chevallier, J. (2001). *Rev. Sci. Instrum.* **72**, 3344–3348.
Nowotny, H. N. & Kieffer, R. (1947). *Metallforschung*, **2**, 257–265.
Payne, A. P., Clemens, B. M. & Brennan, S. (1993). *J. Vac. Sci. Technol. A*, **12**, 598–600.
Peverini, L., Ziegler, E., Bigault, T. & Kozhevnikov, I. (2005). *Phys. Rev. B*, **72**, 045445.
Renaud, G., Ducruet, M., Ulrich, O. & Lazzari, R. (2004). *Nucl. Instrum. Methods Phys. Res. B*, **222**, 667–680.
Ringpfeil, C., Lützenkirchen-Hecht, D. & Frahm, R. (2007). *Thin Solid Films*, **515**, 5597–5600.
Schell, N., Martins, R. M. & Fernandes, F. M. B. (2005). *Appl. Phys. A*, **81**, 1441–1445.
Schell, N., von Borany, J. & Hauser, J. (2007). *AIP Conf. Proc.* **879**, 1813–1816.
Telling, N. D., van der Lann, G., Georgieva, M. T. & Farley, N. R. S. (2006). *Rev. Sci. Instrum.* **77**, 073903.
Thornton, J. A. (1974). *J. Vac. Sci. Technol.* **11**, 666–670.
Vlieg, E., van der Gon, A. W., van der Veen, J. F., Macdonald, J. E. & Norris, C. (1988). *Phys. Rev. Lett.* **61**, 2241–2244.
Vonk, V., Konings, S., Barthe, L., Gorges, B. & Graafsma, H. (2005). *J. Synchrotron Rad.* **12**, 833–834.
Williams, S. M., Yang, H. Q. & Ketterson, J. B. (1991). *Rev. Sci. Instrum.* **63**, 1147–1149.
Willmott, P. R., Schlepütz, C. M., Patterson, B. D., Herger, R., Lange, M., Meister, D., Maden, D., Brönnimann, C., Eikenberry, E. F., Hülsen, G. & Al-Adwan, A. (2005). *Appl. Surf. Sci.* **247**, 188–196.
Zheng, J. Q., Shih, M. C., Wang, X. K., Williams, S., Dutta, P., Chang, R. P. H. & Ketterson, J. B. (1991). *J. Vac. Sci. Technol. A*, **9**, 128–132.